



Effect of Ti, Zr, and Cu content on the microstructure and properties of 2195 Al-Li alloy weldment

S. H. Wen^{1,2} · H. J. Jiao¹ · L. G. Zhou¹ · H. Cheng¹ · S. J. Wu²

Received: 15 August 2022 / Accepted: 5 January 2023 / Published online: 8 February 2023
© International Institute of Welding 2023

Abstract

2195 Al-Li alloy was welded using six kinds of weld filler wires with different contents of zirconium, titanium, and copper. The S2503 weld demonstrated fine α -Al/Al₂Cu/Al₃(Ti, Zr) microstructure and superior mechanical properties. The addition of Zr and Ti refined the grain and modified the solidification mode of the weld metal. With the increase of Ti/Zr addition in the fusion zone, the tensile strength and corresponding elongation of the Al-Li weld increased significantly. The excessive Al₂Cu at the grain boundary helped to alleviate the cracking sensitivity by a “self healing” mechanism, but greatly deteriorated the impact toughness of the weld joint.

Keywords Metals and alloys · Welding · Microstructure · TEM · Mechanical properties

1 Introduction

Lithium (Li) is the lightest metal element with the specific mass of 0.534 g/cm³. With the addition of each 1 wt. % Li, the density of the alloy can be reduced by 3%, while the elastic modulus increased by approximately 6% [1–3]. Aluminum–lithium (Al-Li) alloys have great potential as structural material for aerospace and aircraft applications, due to their low density, high specific strength, and specific stiffness [4–6]. 2195 Al-Li alloy, categorized as Al-Cu-Li-Mg-Ag-Zr,

displays high strength and ductility with good fatigue resistance and corrosion resistance, which was developed at Martin-Marietta and Reynolds. The main precipitation phases such as δ' (Al₃Li), β (Al₃Zr), θ' (Al₂Cu), T₁ (Al₂CuLi), and S' (Al₂CuMg) can be formed during the heat treatment. This high-strength alloy was developed to replace the 2219 alloy for the super lightweight tank (SLWT) of the NASA space shuttle program [4, 7–9], which provided a mass reduction of 3175 kg, increasing almost 50% payload capability for the space shuttle. Consequently, the effects of chemical composition, heat treatment procedure on the microstructure, strengthening mechanism, and mechanical properties of this alloy have been widely investigated [10–15]. Unfortunately, the Al-Li alloy exhibits a poor welding performance, impeding its further application.

The welding property of the Al-Li alloy is very important for the fabrication of the engineering structural component. However, there are some welding problems such as hot cracks and low joint strength coefficient due to the special chemical composition of the Al-Li alloy [16–23]. It is widely known that the welds of the Al-Li alloys are susceptible to cracking during solidification, due to the thermal contraction, solidification shrinkage, and liquidation of phase with low melting point [24–27].

The addition of alloying elements such as Cu or Si to the weld filler wires may help to reduce the crack susceptibility. The 4043 Al-Si weld filler wire was used to weld 2195 Al-Li alloy [20, 28]. It was found that the T (AlLiSi) phase

Highlights

- The 2195 Al-Li weldment consists of α -Al matrix, Al₂Cu phases, and Al₃(Ti, Zr) precipitates.
- The Al₃(Ti, Zr) particles have the main effects of refining the grain size in fusion zone.
- The addition of Ti/Zr and Cu in fusion improves the cracking sensitivity.
- With the increase of Ti/Zr addition in the fusion, the tensile property of the 2195 Al-Li weld increase.

Recommended for publication by Commission XI - Pressure Vessels, Boilers, and Pipelines

✉ S. J. Wu
wusj@buaa.edu.cn

¹ Aerospace Research Institute of Materials & Processing Technology, Beijing 100076, China

² School of Materials Science and Engineering, Beihang University, Beijing 100191, China

formed on the grain boundary of α -Al matrix in fusion zone greatly decreased the crack susceptibility. However, the tensile strength coefficient and the corresponding elongation of 4043 weld joints were quite low [20, 28]. The microstructure and mechanical properties of 2195 welding joint using Al-6Cu weld filler wires were investigated. The 2195/Al-6Cu exhibited a good weld tensile strength, ductility, and fracture properties. Unfortunately, the hot crack susceptibility of the weld joint was still high. In this case, it is necessary to develop new weld filler wires for 2195 Al-Li alloy, which can improve the crack resistance and mechanical properties of the weld joint.

To date, little work has been done to design new weld filler wires for the welding of 2195 Al-Li alloy. The influence of the alloying elements content on crack susceptibility and mechanical properties of the 2195 Al-Li alloy weld is not yet clear. In this study, 2195 Al-Li alloys were welded by tungsten inert gas arc welding. Six types of weld fire wires with different contents of copper, titanium, and zirconium were developed to reduce the cracking susceptibility and improve the mechanical properties. After welding, the microstructure, cracking susceptibility, and mechanical properties of the weld joint were investigated. The effects of Ti, Zr, and Cu content on the microstructure and mechanical performance of the weld joint were discussed.

2 Material and experimental procedures

2.1 Materials

The 8-mm thick hot-rolled commercial 2195-T8 alloy plate was used as base material. The nominal chemical composition (wt. %) of the base material is listed in Table 1. This plate was a solution treated at 500 °C and quenched into water, followed by the cold deformation at 6%, and then artificially aged at 160 °C for 15 h. Six types of weld filler wires were developed to

improve the crack resistance and mechanical properties of the weldment. The weld filler wires with 3.2 mm in diameter were Al based alloys with different contents of zirconium, titanium and copper, identifying as S2501, S2502, S2503, S2504, S2505, and S2506. The nominal chemical composition (wt. %) of weld filler wires are listed in Table 2. For convenience, the weld filler wires with different contents of copper were simply named as Al-6Cu filler and Al-10Cu filler, while those with different contents of titanium and zirconium were simply identified as 0.1% Ti/Zr, 0.2% Ti/Zr, and 0.3% Ti/Zr.

2.2 Welding procedure

The welding specimens were machined to the dimension of 150 mm \times 100 mm \times 6 mm with a single-vee groove joint geometry from the T8 plate. The filler wire dilution was almost 0.6. Before welding, the specimens were soaked in NaOH solution at 60 °C for 3 min, followed by the rinsing with water and HNO₃ solution. The welding area of the specimens was then abraded with steel brush, cleaned with ethanol, and dried in drying oven for 30 min. Tungsten inert gas arc welding (Fronius MW 4000, Austria) was used to join the specimens. Two welding passes were performed with weld fire wires, at 13–16 V welding voltage, 210 A current, and a travel welding speed of 100 mm per minute, using pure Ar gas with 11 L/min flow rate. The wire was added in the molten pool by hand, and the feed rate is almost 20 mm/min.

2.3 Characterization

After welding, the weld joints were cut into small pieces and mounted in the cold-setting resin. X-ray diffraction analysis (XRD, Model AXS-D8, Germany) was performed to identify the phase constitutions in the base material and weld joint using Cu-K α radiation with speed of 6°/min. The differential scanning calorimetry (DSC) was employed

Table 1 The nominal chemical composition (wt. %) of the base material

2195 alloy	Li	Cu	Mg	Zr	Ag	Fe	Si	Zn	Al
	0.8–1.2	3.7–4.3	0.25–0.8	0.08–0.12	0.2–0.4	0.04	0.04	0.02	Bal

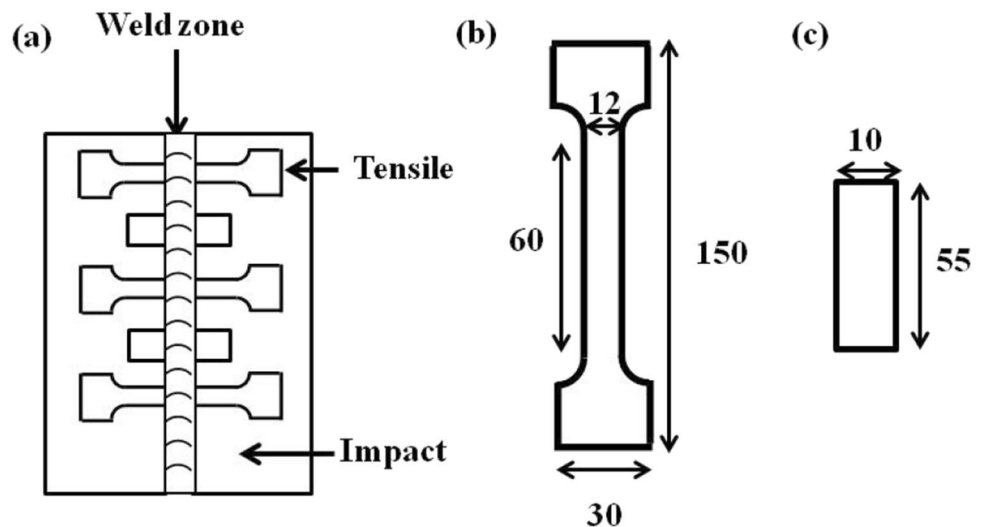
Table 2 The nominal chemical composition (wt. %) of weld filler wires

Filler wire #	Cu	Ti	Zr	Ag	Si	Al
S2501	5.8–6.8	0.08–0.12	0.08–0.12	0.2–0.4	≤ 0.05	Bal
S2502	5.8–6.8	0.18–0.22	0.18–0.22	0.2–0.4	≤ 0.05	Bal
S2503	5.8–6.8	0.28–0.32	0.28–0.32	0.2–0.4	≤ 0.05	Bal
S2504	9.8–10.8	0.08–0.12	0.08–0.12	0.2–0.4	≤ 0.05	Bal
S2505	9.8–10.8	0.18–0.22	0.18–0.22	0.2–0.4	≤ 0.05	Bal
S2506	9.8–10.8	0.28–0.32	0.28–0.32	0.2–0.4	≤ 0.05	Bal

with a differential scanning calorimeter (Model STDQ-600, USA), at a heating rate of 10 °C/min under nitrogen atmosphere. The microstructure of the fusion zone, fusion line, and heat-affected zone were observed using scanning electron microscopy (SEM, Model 200F, Holland) and optical microscope (OM, Model DM4000M, Germany). The chemical composition of the weld joint was determined by energy dispersive spectroscopy (EDS, Oxford Instruments Inc.). Transmission electron microscopy (TEM) was used to further identify the structure of the fusion zone and heat-affected zone.

The mechanical specimens are extracted from different positions of welded joints, as shown in Fig. 1a. Tensile tests of the weld joints with reinforcement were conducted by using CMT-5105 electronic universal material testing machine with loading rate of 2 mm/min at room temperature. The dimension of tensile specimen is shown in Fig. 1b. The relative elongation of the welded joint, determined by the displacement of the moving cross-arm, was used to represent the deformation, and the gauge length was almost 50 mm. The impact tests of weld joint with U-shaped gap were conducted on a digital impact testing machine (HIT 50.PC, Germany). The dimension of impact specimen with 55 mm × 10 mm × 6 mm is shown in Fig. 1c. All tensile and impact test data were found by at least five parallel specimens to obtain the average value. The sensitivity of solidification cracking was analyzed by circular patch test. The circular patch test was used for fully penetrating welds, and a relatively high restraint was imposed on the weld zone transverse to the weld joint. The workpiece of circular weld with 50 mm diameter consists of an inner piece and an outer piece, which is held tightly to the fixture with bolts. The weld specimen was clamped between two copper plates. The details of the circular patch test had been reported by Kou [27].

Fig. 1 Diagram of specimen: **a** extraction position of specimen, **b** dimension of tensile specimen, **c** dimension of impact specimen



3 Results

3.1 Microstructures of the weld joints

Figure 2 shows the X-ray diffraction patterns of the base material and weld joint. The characteristic diffraction peaks of α -Al (PDF#04-0787) and T_1 (Al_2CuLi) (PDF#28-0011) were detected in the base material, meaning that the main strengthening precipitates was T_1 phase. The identified phases in fusion zone were also confirmed by X-ray diffraction, where the peaks of α -Al (PDF#04-0787) and Al_2Cu (PDF#25-0012) were observed.

Typical optical micrographs of the weld joints are shown in Fig. 3. The microstructure showed that the weld joints were divided into the fusion zone (FZ), the fusion line (FL), and the heat-affected zone (HAZ). It can be seen that the

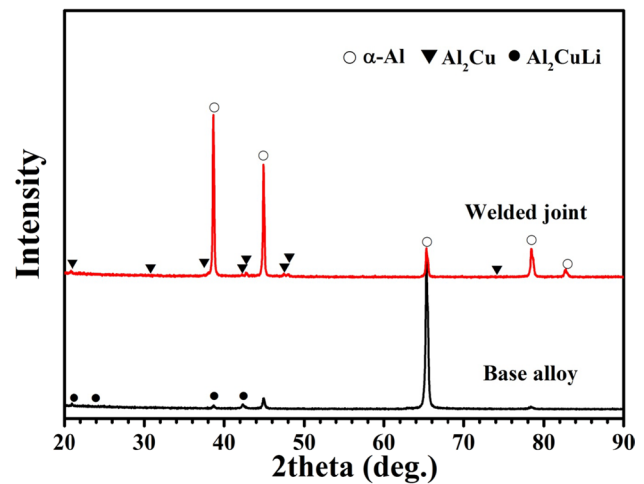
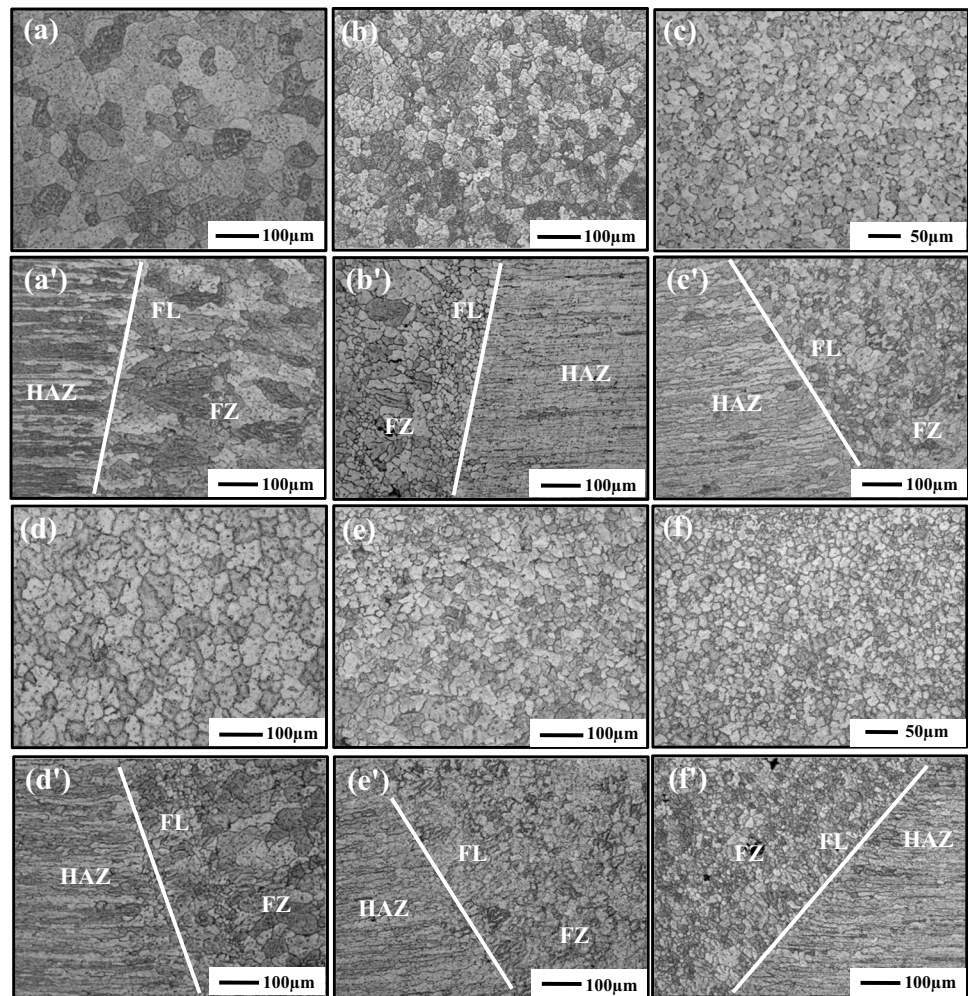


Fig. 2 X-ray diffraction pattern of 2195 Al-Li weld and base alloy

Fig. 3 Optical micrographs of the fusion zone and heat-affected zone in the weldment: S2501 (a) and (a'); S2502 (b) and (b'); S2503 (c) and (c'); S2504 (d) and (d'); S2505 (e) and (e'); S2506 (f) and (f')



microstructure of the S2501 weld represents coarse equiaxed grains in the center of weldment and a columnar dendrite zone adjacent to the fusion line (FL), as seen in Fig. 3a'. With the contents of Ti and Zr increased from 0.1 to 0.3 wt. %, a remarkable decrease on the average grain size from 74 μm to 18 μm for the 2195/Al-6Cu weld, and the average grain size of 2195/Al-10Cu weld decreased from 46 μm to 14 μm . The fine equiaxed grains at the weld interface were not a common occurrence, but Cross thought that the formation of the fine equiaxed grains was due to the Al_3Zr particles released from the fusion metal [29]. This result suggested that the addition of Ti and Zr has significantly effect on grain refinement.

The backscattered electron images in Fig. 4 are performed to observe microstructures of the fusion zone and heat-affected zone in the S2503 and S2506 weld. As shown in Fig. 4a and 4b, the weld joint had a fine and uniform microstructure containing three clearly contrasting phases. The bright Al_2Cu and $\text{Al}_3(\text{Ti}, \text{Zr})$ uniformly dispersed on the Al matrix. The area fractions of the bright Al_2Cu phases were relative to the Cu content in weld filler wires. It was approximately 18.63% in the 2195/Al-10Cu welds, which is

higher than the 12.43% observed in the 2195/Al-6Cu welds. The microstructures of weldments in heat-affected zone are shown in Fig. 4a' and b'. A number of bright phases formed along the grain boundaries in the heat-affected zone.

To further identify the structure of the fusion zone and heat-affected zone in the weld joint, the transmission electron microscopy (TEM) observations were conducted. Figure 5 shows the images of fusion zone in the S2503 weld. The micrograph and corresponding SAED pattern revealed a continuous eutectic Al_2Cu phase distribute at the grain boundary (Fig. 5a and b). The thickness of the eutectic Al_2Cu phase at the grain boundary was almost 0.5 μm . The SAED pattern taken, as seen in Fig. 5d, exhibits that a number of $\text{Al}_3(\text{Ti}, \text{Zr})$ particles and Al_2Cu precipitates dispersed on the Al matrix. Statistical analysis suggested that the sizes of the Al_2Cu precipitates were in the range of 20–100 nm. It was finally confirmed that the main phases in the fusion zone were Al matrix, $\text{Al}_3(\text{Ti}, \text{Zr})$ particles, eutectic Al_2Cu phase, and Al_2Cu precipitates.

The results of TEM analysis at grain boundary in the heat-affected zone are presented in Fig. 6. The

Fig. 4 Backscattered electron images of the fusion zone and heat-affected zone in the S2503 weldment (a) and (a') and S2506 weldment (b) and (b')

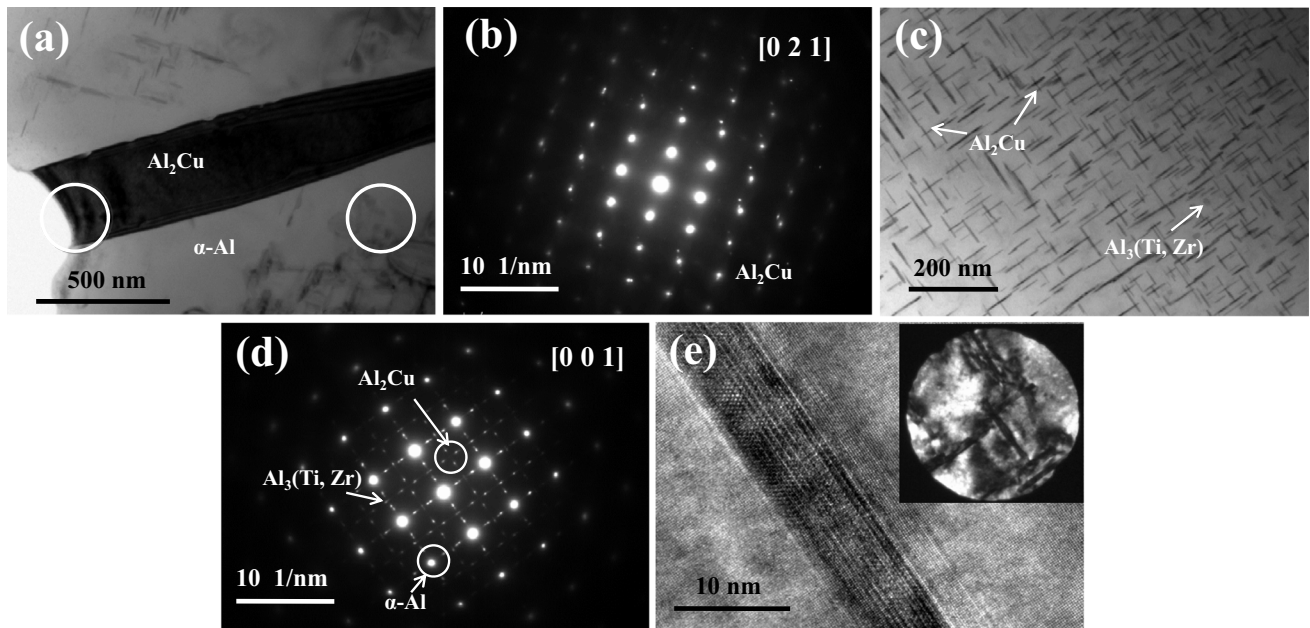
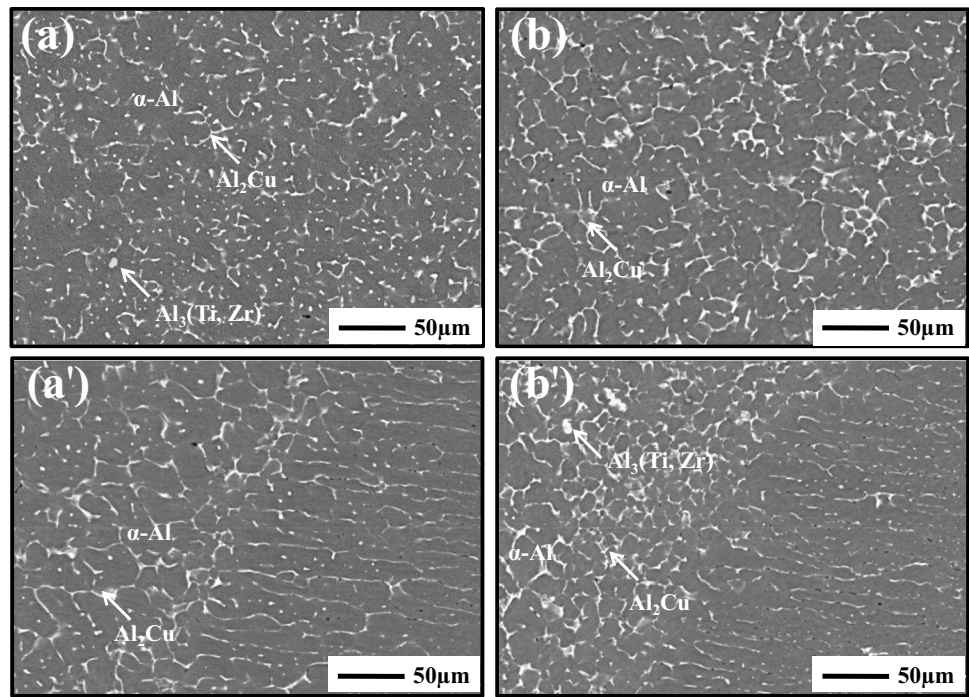


Fig. 5 TEM images of the fusion zone in the S2503 weld: **a** image of grain boundary along $\langle 0\ 2\ 1 \rangle$, **b** corresponding SAED pattern, **c** image of precipitates taken along $\langle 0\ 0\ 1 \rangle_{Al}$ direction, **d** corresponding SAED pattern, **e** HRTEM image of the plate phase

discontinuous and coarse particles were observed at the grain boundary. The SAED pattern suggests that this coarse particle consists of T_B (Al_7Cu_4Li), as seen in Fig. 6d. This result was in good agreement with the research of the weld heat-affected zone simulation by Chen [20]. Figure 7 shows the TEM micrographs and

corresponding SAED pattern of the strengthening precipitates in the heat-affected zone. The sphere particles of δ' (Al_3Li) with the size of 200 nm are observed in Fig. 7a. The micrograph and SAED pattern along $\langle 0\ 0\ 1 \rangle_{Al}$ direction show that the needle-like T_1 phase dispersed on matrix [30], as seen in Fig. 7b. In addition, a small number

Fig. 6 TEM images of the grain boundary in the heat-affected zone: **a** image of heat-affected zone along $\langle 001 \rangle$, **b** image of grain boundary microstructures, **c** image of coarse particle at grain boundary, **d** corresponding SAED pattern

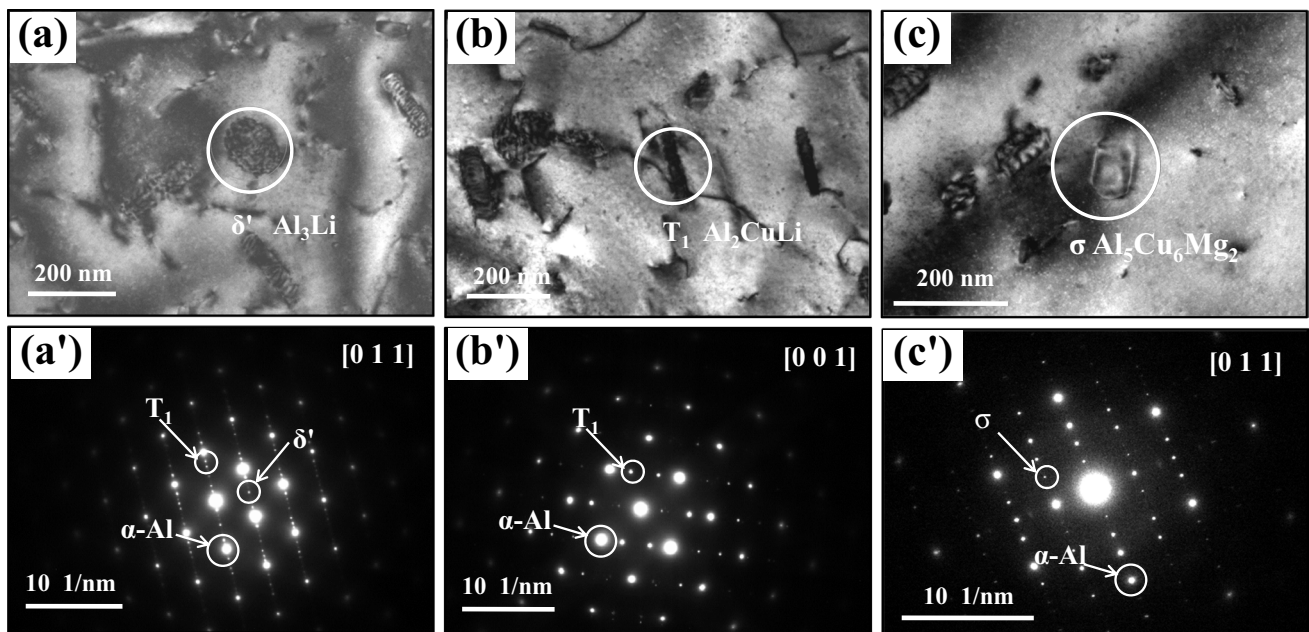
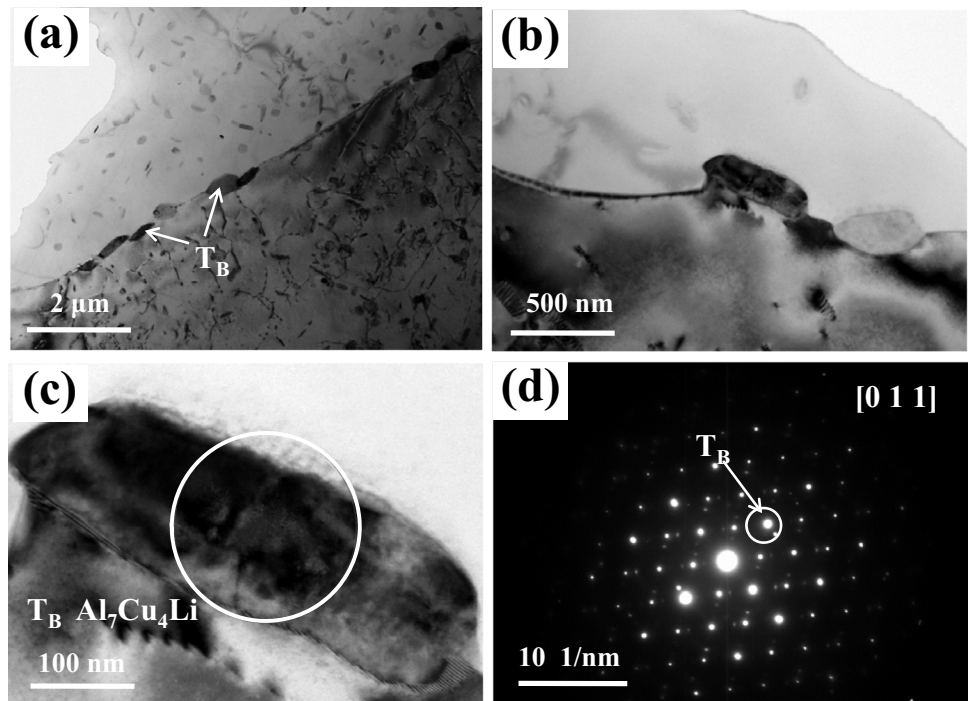


Fig. 7 TEM images of precipitates in the heat affected zone: **a** and **a'** image of Al_3Li particles along $\langle 001 \rangle$ and corresponding SAED pattern, **b** and **b'** image of Al_2CuLi particles along $\langle 001 \rangle$ and cor-

responding SAED pattern, **c** and **c'** image of $\text{Al}_5\text{Cu}_6\text{Mg}_2$ particles along $\langle 011 \rangle$ and corresponding SAED pattern

of cubic precipitates were speculated as σ ($\text{Al}_5\text{Cu}_6\text{Mg}_2$) phase. Thus, the microstructure of the heat-affected zone was finally confirmed to be sphere particles δ' , plates T_B , needle-like T_1 , and cubic precipitate σ dispersed on α -Al matrix.

3.2 Weld cracking susceptibility

The circular patch test was conducted to analyze the cracking susceptibility, and the sum of crack length on the circular patch served as the index of cracking sensitivity. X-ray

radiographs of the circular patch specimens are presented in Fig. 8. It was clear that the continuous cracks could be observed at the weld periphery. As shown in Fig. 8a, the S2501 weld exhibits a poor cracking susceptibility; i.e., the crack length on the circular patch reaches approximately 11 mm, while the crack length of S2503 and S2506 weld decreases to 1–2 mm. The crack length as a function of average grain size in weld joint is plotted in Fig. 9. The linear relationship between maximum crack length of the welds and the average grain size with the same Cu content further suggested that the addition of Ti and Zr improved crack resistance. The maximum crack length of the S2504 weld was 5.3 mm, while that of the S2505 and S2506 weld was 2.6 mm and 1.1 mm, respectively. The linear rate constant k for the cracking susceptibility of the weldment can be calculated according to the equation:

$$L = k \cdot d \tag{1}$$

where L (mm) is the maximum crack length on circular patch specimens and d (μm) is the average grain size in fusion zone. The k value increased with decreasing nominal Cu content in the weld, which were 113 for the Al-6.4Cu weld metal and 151 for Al-4.8Cu weld metal. In conclusion, the crack lengths on the circular patch of the S2503, S2505, and S2506 welds were 2.4 mm, 2.6 mm, and 1.1 mm, respectively, which revealed a good performance in crack resistance.

3.3 Mechanical properties

The tensile tests are carried out for the weld joints with different weld filler wires at the room temperature, and the

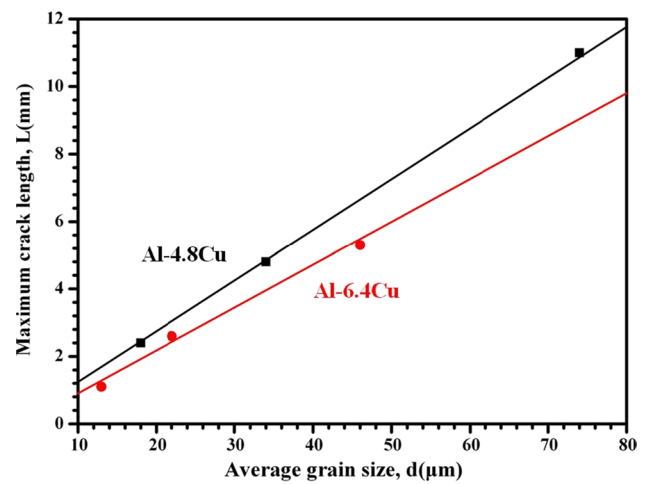


Fig. 9 Maximum crack length as a function of average grain size in the weld joint

average measurements of the tensile strength (MPa) and corresponding elongation (%) are given in Table 3. The tensile strength of the weld joints was about 60.4–68.2% of the base material. The test results in Table 3 demonstrate that the tensile strength and elongation of the welds increased with the increase of the Ti and Zr content. By comparing the results of specimens S2502 with S2505 and S2503 with S2506, it can be found that the effect of Cu content on the tensile strength of the weld was not significant, but the elongation of the weld slightly decreased with the increase of Cu content.

In order to investigate the relationship between the mechanical properties and the microstructures of the weld joint, the

Fig. 8 X-ray radiographs of the circular patch specimens S2501–S2506 (a)–(f)

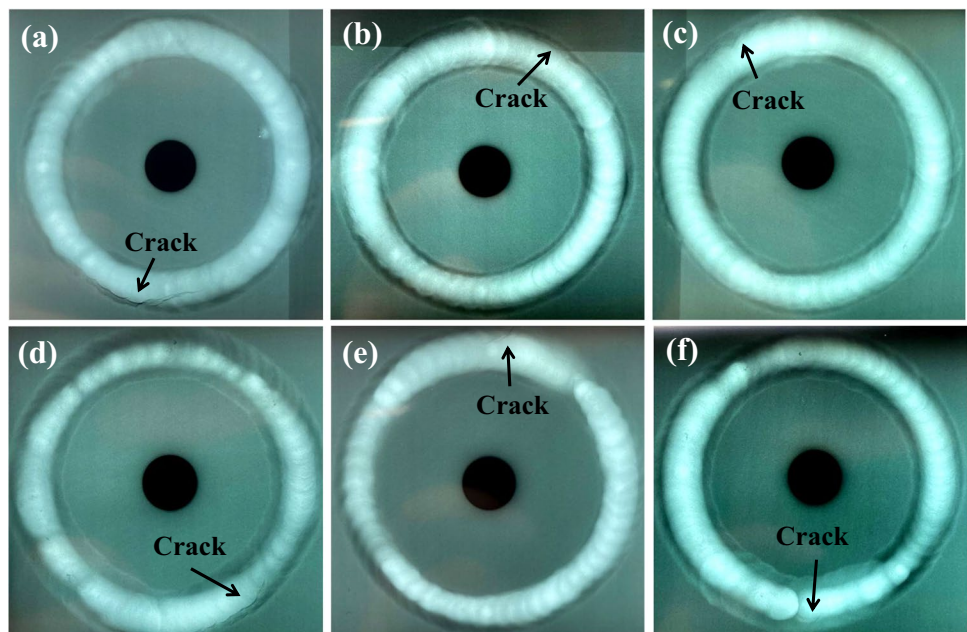


Fig. 10 SEM micrographs of the tensile fracture surfaces: **a** S2503 weldment and **b** S2506 weldment

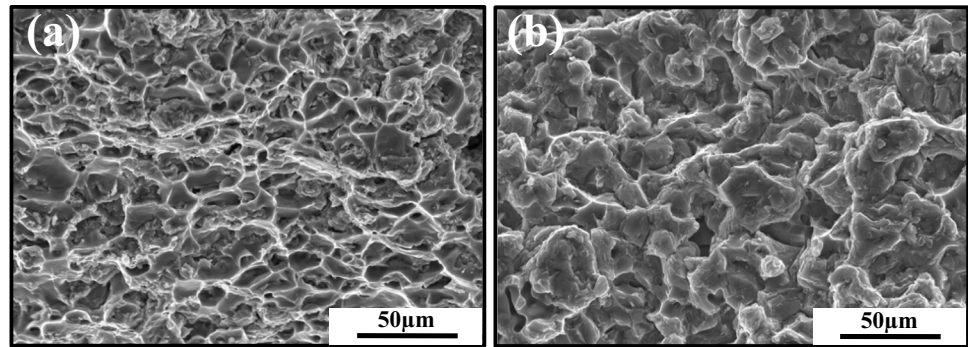


Table 3 Tensile properties of the 2195 Al-Li welded joint

Filler wire #	Ultimate tensile strength, MPa	Elongation, Pct
S2501	338.5	3.6
S2502	362.1	4.3
S2503	382.7	5.5
S2504	346.1	2.5
S2505	360.3	3.3
S2506	376.8	4.0

tensile fracture surfaces were observed. Figure 10 shows the SEM images of the tensile fracture surfaces of the weld joint. The weld joints ruptured inside the fusion line during stretching process. For the S2503 weld, the deep and small dimples filled up the fractured Al grains, which demonstrated that the plastic deformation occurred before fracture. In contrast, a number of shallow dimples are covered on fracture surface in the S2506 weld, as seen in Fig. 10b. Consequently, it can be concluded that the S2503 weld displayed the best tensile properties.

Table 4 lists the impact toughness (α_k) of the weld joint as a function of the nominal Cu and Ti/Zr content. The effect of Ti/Zr content on impact toughness was contrary to the tensile strength. With the increased of Ti and Zr content, the impact toughness of the weld joint slightly decreased. It can be seen that the impact performance of the 2195/Al-10Cu weld was poor, and the impact toughness values were lower

Table 4 Impact properties of the 2195 Al-Li welded joints

Filler wire #	Fracture toughness, J/cm ²
S2501	20.5
S2502	19.9
S2503	19.4
S2504	9.6
S2505	8.2
S2506	6.7

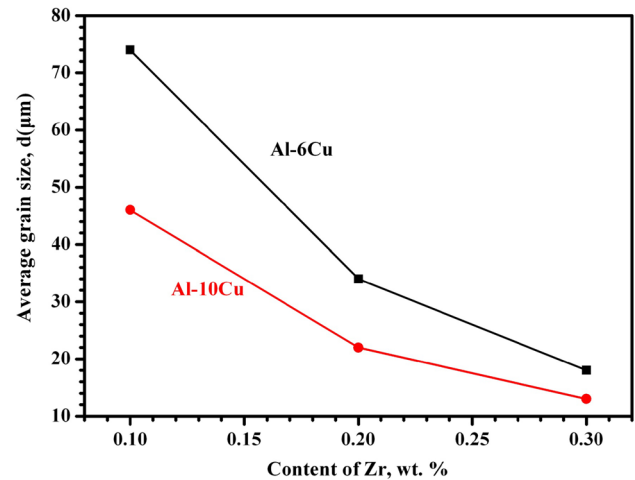


Fig. 11 Average grain size in the fusion zone as function of Ti/Zr content in the weld filler wires

than 10 J/cm², while the impact toughness of the 2195/Al-10Cu weld reached approximately 20.0 J/cm². This result showed that the excessive addition of Cu substantially deteriorated the impact toughness of the weldment.

4 Discussion

4.1 Effect of Ti and Zr content on the microstructure of weldment

As observed in Fig. 3, the statistical analysis reveals that the grain size of the fusion zone is related to the nominal Ti and Zr contents. Figure 11 shows the average grain size in fusion zone as function of Ti/Zr content in weld filler wire. The crystal growth rate for a given undercooling is inversely proportional to the growth restriction parameter Q . Easton [31] reported a relationship of the growth restriction parameter Q to the solutes content by the following equation:

$$Q = m(k - 1)C_0 \quad (2)$$

where k is the solute partition coefficient, m is the slope of liquidus, and C_0 is the solutes content in the alloy molten. The overall growth restriction parameter is the sum of the Q values for the individual solutes. Thus, the grain size related to the crystal growth rate is controlled by Ti and Zr content.

With the increase of Ti and Zr contents in the weld filler wires, the grain size of the α -Al decreases remarkably [32], and the morphology of α -Al gradually transforms into the fine equiaxed grain, as shown in Figs. 3 and 11. As the effective nucleation sites, Ti/Zr dispersoids are initially present in the filler wire, when set in the molten, and have a strong capacity to modify the grains in weldment, as seen in Fig. 3. According to this nucleation theory, the refinement of the nucleant particles increases the amount of potential solidification sites and promotes the formation of the finer equiaxed grains in the fusion zone [33]. Consequently, the addition of Ti/Zr in the weld can

effectively refine the grains and modify the solidification of the weld joint.

4.2 The relationship between the composition and cracking susceptibility

In this work, the circular patch test is conducted to analyze the cracking susceptibility, and the sum of crack length on the circular patch serves as the index of cracking sensitivity. X-ray radiographs of the circular patch specimens show that the solidification cracking occurs along the center of the weld. The RDG model [26] shows that the cracking behavior in the solidification process is mainly determined by three factors: the tensile stress between grains (crack driving force), the deformation ability between grains (crack resistance), and the liquid compensation capacity along the grain boundaries (crack resistance).

The fitted linear relationship between crack length and the average grain size in the fusion zone further suggests that the excessive Cu improved crack resistance. This phenomenon

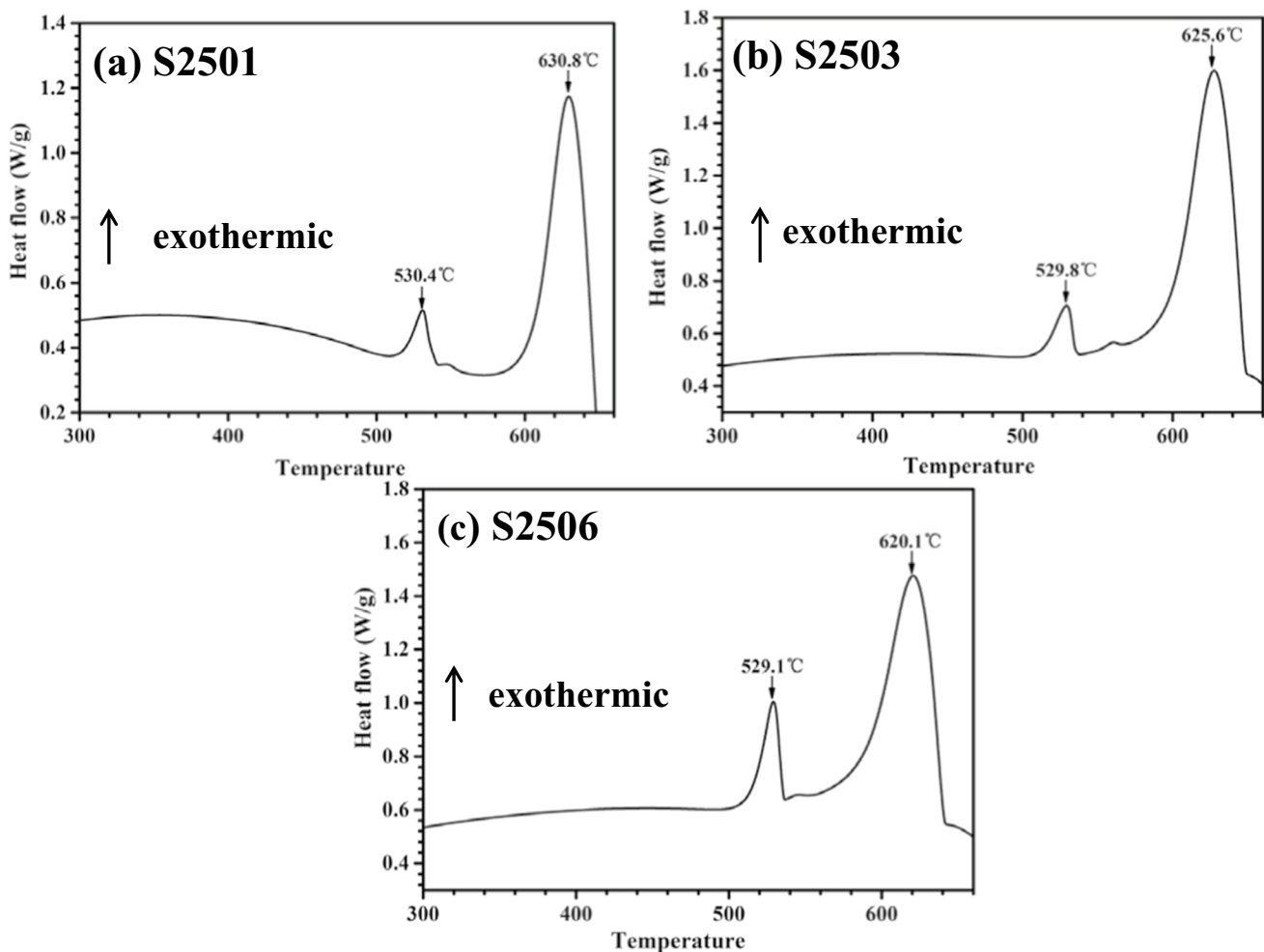


Fig. 12 DSC curves of 2195 Al-Li weld joints: S2501 weldment (a), S2503 weldment (b), and S2506 weldment (c)

can be explained by the theory of “self healing.” The eutectic Al_2Cu liquid at grain boundary can be sufficient to heal the incipient cracks during the solidification process. In addition, the fine equiaxed grain structure is easier to deform than coarse columnar grain structure, which can also improve the crack resistance, as shown in Figs. 8 and 9.

The solidification temperature range, as an important tensile stress factor, has been known to affect the susceptibility of solidification cracking. To identify the solidification temperature range of the weld metal, the differential scanning calorimetry (DSC) is conducted. Figure 12 illustrates the DSC curves of the heat flow as a function of the temperature in cooling process. The solidification temperature range of the weld metal can be calculated by the following equation:

$$T_r = T_i - T_f \quad (3)$$

where T_r is the solidification temperature range, T_i is the initial crystallization temperature, and T_f is the final crystallization temperature. The solidification temperature ranges of the weld metal and base material are listed in Table 5. The solidification temperature range of the base material was 117.2 °C, while that of the S2503 and S2506 weld decreased to 95.8 °C and 91.0 °C. Previous works verified that the wide solidification temperature range is susceptible to solidification cracking, due to the larger (S + L) region in the weld metal or the mushy zone [32]. In conclusion, the crack resistance of the weld joint improved by increasing the contents of Cu, Ti, and Zr.

4.3 The relationship between the composition and mechanical properties

The tensile and impact tests were carried out for weld joints with different weld filler wires at room temperature. The joints ruptured in the fusion zone adjacent to the fusion line, which means that the fusion zone is the weakest region compared with the heat-affected zone and base material. Previous research has shown that T_1 precipitates have a greater strengthening effect than other strength phases in Al-Cu-Li alloys [34, 35]. The observation of microstructures confirms that the main strengthening phase in the fusion zone was

Table 5 Solidification temperature range of the weld metal and the base material

Material states	Solidification temperature range (ΔT), °C
2195 base material	117.2
S2501 weld	100.4
S2503 weld	95.8
S2506 weld	91.0

Al_2Cu and no T_1 precipitate was found in the weld joint, as shown in Figs. 4 and 5. Therefore, the strength of fusion zone is weaker than that of the heat-affected zone and base material.

In this work, the relationship between the tensile strength and the grain size ($D^{-1/2}$) of the weldments is consistent with the Hall–Petch equation [36]:

$$\sigma_b = \sigma_0 + k_b D^{-1/2} \quad (4)$$

where σ_b is tensile strength, σ_0 is the Peierls-Nabarro stress, D is the grain size of the weldment, and k_b is the slope. The tensile strength of the weldments plotted against grain size ($D^{-1/2}$) is shown in Fig. 13. The k_b value was 230.8 $\text{Mpa}\cdot\mu\text{m}^{-1/2}$ for 2195/Al-10Cu weldments and 375.0 $\text{Mpa}\cdot\mu\text{m}^{-1/2}$ for 2195/Al-6Cu weldments. These results showed that the tensile strength and the corresponding elongation of the weld joint increased with the increase of Ti and Zr contents. However, the addition of Al_3 (Ti, Zr) particles in the fusion zone slightly reduced the toughness of the weld joint. In addition, once the excessive Al_2Cu was formed at the grain boundary, the plastic deformation of the grain boundary will be reduced, resulting in poor plasticity and toughness properties of the weld joint. Therefore, the impact toughness and elongation of the weldment decreased with the increase of the nominal Cu content.

5 Conclusions

The effects of Ti, Zr, and Cu content on microstructure, cracking susceptibility, and mechanical behavior of 2195 Al-Li alloy weld were investigated using six kinds of weld filler wires. It can be concluded with the following points.

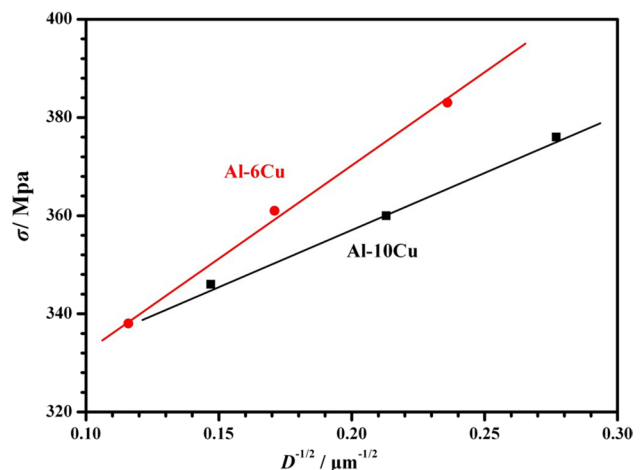


Fig. 13 Tensile strength (σ) of the weldments plotted against the grain size ($D^{-1/2}$)

- 1) The microstructure of the fusion zone consists of α -Al matrix, eutectic and precipitate Al_2Cu phases, and $\text{Al}_3(\text{Ti}, \text{Zr})$ particles, while the sphere particles δ' (Al_3Li), plates $\text{T}_B(\text{Al}_7\text{Cu}_4\text{Li})$, and $\text{T}_1(\text{Al}_2\text{CuLi})$, cubic precipitate $\sigma(\text{Al}_5\text{Cu}_6\text{Mg}_2)$ are located in the heat effect zone. The fractions of Al_2Cu and $\text{Al}_3(\text{Ti}, \text{Zr})$ are relative to the content of Cu, Ti, and Zr in fusion.
- 2) The $\text{Al}_3(\text{Ti}, \text{Zr})$ particles have the main effects of acting as heterogeneous nucleation sites for aluminum grains, which refine the grain size in fusion zone.
- 3) The quantity of Al_2Cu phase at grain boundary and the grain size in fusion zone play a key role in the cracking sensitivity of 2195 Al-Li weld. Therefore, the addition of Ti/Zr and Cu in fusion improves the crack resistance of the weld joint.
- 4) With the increase of Ti/Zr addition in the fusion zone, the tensile strength and corresponding elongation of 2195 Al-Li weld increase, while the impact toughness slightly decreases. An excessive Al_2Cu at the grain boundary greatly deteriorates the impact toughness of weld joint.
- 5) The S2503 filler with the nominal chemical compositions (wt. %) of Al-6Cu-0.3Ti-0.3Zr-0.3Ag displayed the best tensile properties.
6. EL-Aty AA, Xu Y, Guo X et al (2018) Strengthening mechanisms, deformation behavior, and anisotropic mechanical properties of Al-Li alloys: a review. *J Adv Res* 10:49–67
7. Williams JC, Starke EA (2003) Progress in structural materials for aerospace systems. *Acta Mater* 51:5775–5799
8. Dursun T, Soutis C (2014) Recent developments in advanced aircraft aluminium alloys. *Mater Des* 56:862–871
9. Nayan N et al (2015) Microstructure and micro-texture evolution during large strain deformation of an aluminium-copper-lithium alloy AA2195. *Mater Des* 65:862–868
10. Nayan N et al (2013) George, Ambient and cryogenic tensile properties of AA2195-T87 sheets with pre-aging cold work by a combination of cold rolling and stretching. *Mater Sci Eng A* 585:475–479
11. Kim JH, Jeun JH et al (2016) Effect of precipitates on mechanical properties of AA2195. *J Alloy Compd* 669:187–198
12. Nayan N et al (2014) Sharma, Mechanical properties of aluminium-copper-lithium alloy AA2195 at cryogenic temperatures. *Mater Des* 58:445–450
13. Suresh M, Sharma A, More AM, Nayan N, Suwas S (2018) Effect of scandium addition on evolution of microstructure, texture and mechanical properties of thermo-mechanically processed Al-Li alloy AA2195. *J Alloy Compd* 740:364–374
14. Hekmat-Ardakan A, Elgallad EM, Ajersch F, Chen XG (2012) Microstructural evolution and mechanical properties of as-cast and T6-treated AA2195 DC cast alloy. *Mater Sci Eng A* 558:76–81
15. Wang YX, Zhao GQ et al (2018) Microstructures and mechanical properties of spray deposited 2195 Al-Cu-Li alloy through thermo-mechanical processing. *Mater Sci Eng A* 727:78–89
16. Zhang XY, Huang T, Yang WX, Xiao RS, Liu Z, Li L (2016) Microstructure and mechanical properties of laser beam-welded AA2060 Al-Li alloy. *J Mater Process Technol* 237:301–308
17. Solórzano IG, Darwish FA, de Macedo MC, de Menezes SO (2003) Effect of weld metal microstructure on the monotonic and cyclic mechanical behavior of tig welded 2091 Al-Li alloy joints. *Mater Sci Eng A* 348:251–261
18. Reddy GM, Gokhale AA (2002) Effect of the ratio of peak and background current durations on the fusion zone microstructure of pulsed current gas tungsten arc welded Al-Li alloy. *J Mater Sci Let* 21:1623–1625
19. Zhao L, Wang SG, Jin Y, Chen Y (2018) Microstructural characterization and mechanical performance of Al-Cu-Li alloy electron beam welded joint. *Aerosp Sci Technol* 82–83:61–69
20. Chen DL, Chaturvedi MC (2011) Effects of welding and weld heat-affected zone simulation on the microstructure and mechanical behavior of a 2195 aluminum-lithium alloy. *Metall and Mater Trans A* 32:2729–2741
21. Chen K, Yang WX, Xiao RS (2011) Direct laser welding of an Al-Li alloy plate with-out prior surface cleaning. *Laser Eng* 22:361–369
22. Kostrivas A, Lippold J (1999) Weldability of Li-bearing aluminium alloys. *Inter Mater Rev* 44:217–237
23. Jeffrey HS (1996) Investigation of grain boundary chemistry in Al-Li 2195 welds using Auger electron spectroscopy. *Thin Solid Film* 277:121–127
24. Liu JW, Kou S (2016) Crack susceptibility of binary aluminum alloys during solidification. *Acta Mater* 110:84–94
25. Soysal T, Kou S (2019) Effect of filler metals on solidification cracking susceptibility of Al alloys 2024 and 6061. *J Mater Pro Technol* 266:421–428
26. Liu JW, Duarte HP, Kou S (2017) Evidence of back diffusion reducing cracking during solidification. *Acta Mater* 122:47–59
27. Kou S (2003) Solidification and liquation cracking issues in welding. *JOM* 55:37–42

Declarations

Conflict of interests The authors declare no competing interests.

Disclaimer We also declare that we do not have any commercial or associative interest that represents a conflict of interest in connection with the work entitled “Effect of Ti, Zr and Cu content on the microstructure and properties of the 2195 Al-Li alloy weldment”.

References

1. Rioja RJ (1998) Fabrication methods to manufacture isotropic Al-Li alloys and products for space and aerospace applications. *Mater Sci Eng A* 257:100–107
2. Gupta RK, Nayan N, Nagasireesha G, Sharma SC (2006) Development and characterization of Al-Li alloys. *Mater Sci Eng A* 420:228–234
3. Pedemonte M, Gambaro C, Lertora E, Mandolfi C (2013) Fatigue assessment of AA 8090 friction stir butt welds after surface finishing treatment. *Aerosp Sci Technol* 27:188–192
4. Rioja RJ, Liu J (2012) The evolution of Al-Li base products for aerospace and space applications. *Metall Mater Trans A* 43:3325–3337
5. Decreusa B, Deschamps A et al (2013) The influence of Cu/Li ratio on precipitation in Al-Cu-Li-x alloys. *Acta Mater* 61:2207–2218

28. R Jan, PR Howell, RP Martukanitz (1996) Optimizing the parameters for laser beam welding of aluminum-lithium alloy 2195, Proceedings of 4th International Conference on Trends in Welding Research, ASM International, Ohio, 329–334
29. CE CROSS (2022) Applying solidification theory to aluminum weldability and consumable development [J]. *Welding Journal* 101
30. Zhang QY, Zhang CS, Lin J, Zhao GQ, Chen L, Zhang H (2019) Microstructure analysis and low-cycle fatigue behavior of spray-formed Al-Li alloy 2195 extruded plate. *Mater Sci Eng A* 742:773–787
31. Easton MA, StJohn DH (1999) Grain refinement of aluminium alloys. *Metall Mater Trans A* 30(6):1613
32. S Kou (2013) *Welding metallurgy*, seconded., John Wiley and Sons, Hoboken, 257–300
33. Atamanenko TV, Eskin DG, Sluiter M, Katgerman L (2016) On the mechanism of grain refinement in Al-Zr-Ti alloys. *J Alloy Compd* 669:187–198
34. Rodgers BI, Prangnell PB (2016) Quantification of the influence of increased prestretching on microstructure-strength relationships in the Al-Cu-Li alloy AA2195. *Acta Mater* 108:55–67
35. Gable B (2001) The role of plastic deformation on the competitive microstructural evolution and mechanical properties of a novel Al-Li-Cu-X alloy. *J Light Met* 1:1–14
36. Li XW, Cai QZ, Zhao BY, Xiao YT, Li B (2016) Effect of nano TiN/Ti refiner addition content on the microstructure and properties of as-cast Al-Zn-Mg-Cu alloy. *J Alloy Compd* 675:201–210

Publisher's note Springer Nature remains neutral with regard to jurisdictional claims in published maps and institutional affiliations.

Springer Nature or its licensor (e.g. a society or other partner) holds exclusive rights to this article under a publishing agreement with the author(s) or other rightsholder(s); author self-archiving of the accepted manuscript version of this article is solely governed by the terms of such publishing agreement and applicable law.